

Boron diffusion in extrinsically doped crystalline siliconD. De Salvador, E. Napolitani, G. Bisognin, M. Pesce, and A. Carnera
*MATIS CNR-INFN and Dipartimento di Fisica, Università di Padova, Via Marzolo 8, 35131 Padova, Italy*E. Bruno, G. Impellizzeri, and S. Mirabella
MATIS CNR-INFN and Dipartimento di Fisica e Astronomia, Università di Catania, Via S. Sofia 64, 95123 Catania, Italy

(Received 31 July 2009; published 29 January 2010)

Boron diffusion is investigated in details by monitoring B-sharp concentration profiles embedded in isoconcentration doping backgrounds. Atomistic diffusion parameters (kick-out rate g , mean-free path of the mobile species λ , and the diffusivity D) are experimentally evaluated as a function of temperature and doping level both of p or n type. This allows for a quantitative determination of the physical phenomena involved in the B diffusion process. We found that negatively charged substitutional B diffuses by interaction with neutral or doubly positively charged self-interstitials. The BI complex formed after interaction diffuses mainly in a neutral state and, to a less extent, through singly negatively charged state. The former contributes for about one tenth to the full diffusion in intrinsic condition at 700 °C whereas it plays a significant role in high n -codoping regime. Moreover, n codoping with As or P induces a Coulomb pairing between the different charge states of the dopants that reduces diffusion. Pairing effect is disentangled by the effect of BI⁻ diffusion and pairing energies are determined for both As and P presence. The resulting quantitative model of diffusion is presented and compared with existing literature.

DOI: [10.1103/PhysRevB.81.045209](https://doi.org/10.1103/PhysRevB.81.045209)

PACS number(s): 61.72.jj, 66.30.J-, 66.30.Pa, 61.72.uf

I. INTRODUCTION

Boron diffusion in crystalline silicon has been widely investigated for more than 40 years (see, for example, the review in Ref. 1, and references therein) since of its technological interest as the main used p -type dopant in Si-based microelectronics.

B diffusion has very peculiar diffusion features that go beyond the Fick's laws. B diffuses through the interaction with self-interstitial point defects (I 's) by the formation of a BI complex that can move into the lattice.²⁻⁷ This fact was demonstrated by studying the diffusion shape of sharp B layers (delta-doping layers) evidencing non-Fickian exponential tails. The extension of these tails is related to the BI mean-free path λ .^{4,5} Moreover, the I -mediated diffusion mechanism makes B diffusivity very sensitive to the I concentration; the frequency g with which diffusion events (i.e., BI formation) are generated is proportional to the I concentration. Therefore, nonequilibrium processes such as oxidation (oxidation-enhanced diffusion) and ion implantation (transient-enhanced diffusion), heavily affect B diffusion since they increase the I concentration.⁷ B-enhanced diffusion has detrimental effects for ultrashallow junctions formation, thus a clear comprehension of the diffusion microscopic mechanisms is fundamental. In this context, B delta doping grown by molecular-beam epitaxy (MBE) can be usefully employed to investigate the above phenomena since the high-concentration gradients of these structures make the experiments very sensitive to diffusion (see, for example, Refs. 8-10).

A second fundamental aspect of B diffusion is its relation with the free-carrier concentration or, in other terms, with the Fermi-level position. It is well assessed by about 40 years that B diffusion linearly increases with holes (h) concentration in a wide range of temperatures (870-1250 °C).¹¹⁻¹³ This phenomenon causes the enhancement of B diffusivity

by increasing the B concentration and thus the h concentration. This fact is more relevant in current junction fabrication where B-active concentrations reaches very high levels.

Putting together these two aspects (I -mediated and h -mediated diffusion) in a single physical comprehension has been the topic of many recent papers. First attempts were performed by theoretical studies¹³⁻¹⁷ that showed, by *ab initio* calculations, how I and BI species with different charge states are involved in the diffusion process and suggesting an interaction between free carriers and the structural protagonists of B diffusion (I and BI). More in details, it was demonstrated that the structure, the formation energy, and the migration barrier of these species strongly depend on their charge state. Neutral, negatively, and positively charged BI complexes were considered but a general consensus on what is the most relevant complex for diffusion has not been yet established from a theoretical point of view.

Only very recently experimental data able to fix the interplay among I , BI (in their different charge states), and the free charges were available.^{18,19} In Ref. 18 we measured the frequency of migration events g , the BI mean-free path λ , and the diffusivity as a function of the hole concentration from about intrinsic to largely p -doped regime.¹⁸ The experimental approach we used, and that we further exploited in the present paper, is based on the accurate characterization of a B delta²⁰ embedded in a isotopically different B homogeneous backgrounds that independently change the doping level (see also Sec. II). These data (that are reported in Sec. IV together with the new data in n -type regime that are object of this work), are well fitted by the following equations:

$$g = g_{I0} + g_{I++} \left(\frac{p}{n_i} \right)^2, \quad (1)$$

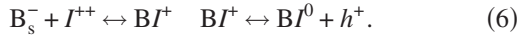
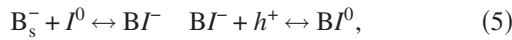
$$D = D_{BI0} \frac{p}{n_i}, \quad (2)$$

$$\lambda = \sqrt{\frac{D_{B/I^0} \frac{p}{n_i}}{g_{I^0} + g_{I^{++}} \left(\frac{p}{n_i}\right)^2}}. \quad (3)$$

The frequency g is reproduced by a constant plus a quadratic term [Eq. (1)] as a consequence of B_s^- (the negatively charged substitutional B) interaction with neutral I^0 (whose population does not depend on p/n_i) and doubly charged I^{++} (whose population increases with the square of p/n_i). These two interactions are the initial step of the diffusion mechanism, and produce the BI^- and BI^+ complexes, respectively. The linear trend of D vs hole concentration [Eq. (2)] implies that the net charge balance for diffusion involves one singly positively charge. As a consequence, BI^0 is the dominant mobile species and BI^- and BI^+ have to, respectively, get and lose one hole before moving. Finally λ 's modeled by Eq. (3) that is derived from Eqs. (1) and (2) and the general formula between D , g , and λ (Ref. 4),

$$D = g\lambda^2. \quad (4)$$

Therefore the experiment in Ref. 18 proposed the following reaction chains to explain diffusion in intrinsic and p -doping regime:



This picture was more recently confirmed by an independent experimental approach by Bracht *et al.*¹⁹ In their work B was diffused by a surface source into an epitaxial layer having Si isotopically enriched markers allowing for simultaneously determination of Si self-diffusion together with B diffusion. The broad B profiles are not sensitive to the mean-free path of the BI species and only allow for B average diffusion determination, moreover the doping is not independently changed by means of isotopic background but diffusing B itself progressively dopes the layer. On the other hand, having access to the self-diffusion, the Bracht's approach allows to estimate the change in I population due to doping. Self-diffusion is sensitive also to vacancy (V) component and the I population information can only be determined by a cross fitting with other diffusing-doping species that enhance the V population. The results of Bracht and co-worker confirm that I^0 , I^{++} , and BI^0 are the species responsible for B diffusion in p -doped regime. The investigation was performed in the temperature range between 850 and 1100 °C and allowed for the determination of temperature dependence and energetic of the I transport capacities and B diffusivity.

Recently Windl^{21,22} compared the experimental results mentioned above^{18,19} with *ab initio* calculations, evidencing a substantial agreement among theory and experiments. Quite surprisingly, he concluded that I^+ has the lower energy cost with respect to I^0 and I^{++} . The problem is that at temperatures at which the experiments are performed and diffusion really occurs, both entropic prefactor and energy cost play a role to determine diffusion parameters according to an

Arrhenius trend. In the range from 700 to 1100 °C, experimental data^{18,19} demonstrate that I^0 and I^{++} dominate B diffusion and it may be that this is due to a very low prefactor for I^+ despite the low-energy cost of this species. This is exactly what data of Ref. 19 suggest even if with a very large error bar in qualitative agreement with theoretical predictions for energy barriers but a theoretical evaluation of prefactor should be performed to complete the comparison.

In the present paper we reported a recent development of our investigation with isoconcentration experiments on B delta doping that allows to extend and complete the experimental picture reported above.

In the first part of the paper (Sec. III) we have investigated the temperature dependence of the model described by Eqs. (1)–(3) in order to determine the energetics of g_{I^0} , $g_{I^{++}}$, and D_{B/I^0} . In the second part of the paper (Sec. IV) we have extended the description of the B diffusion mechanism to the n -type doping regime by adding As and P backgrounds to the B delta. We will show that a small diffusivity of BI^- has to be assumed to explain the data and that, at the same time, Coulomb attraction between donor and acceptor (pairing) has to be considered.

Putting together the results of the last two sections a comprehensive quantitative model for B diffusion as a function of temperature and doping (both p and n type) is obtained.

II. EXPERIMENT

Similarly to what performed in Ref. 18, the basic idea of the experiment is to analyze the diffusion of a sharp ^{11}B spike suitable for the simultaneous determination of λ and g , embedded in different doping backgrounds. The Si samples were grown by MBE with a B spike (at the depth of 180 nm, using a natural isotopic abundance solid B source) and a $\text{Si}_{1-x}\text{C}_x$ alloy layer between 390 and 440 nm with $x = 0.3$ at. %. Subsequently the samples were amorphized down to a depth of 500 nm by multiple energy Si-ion implantations.

Multiple ^{10}B implants were then performed to embed the ^{11}B spike in a p -type background with a concentration of about 2.8×10^{19} B/cm³ constant within $\pm 5\%$ in the range between 80 and 320 nm. In order to explore B diffusion in n -doping conditions some samples were processed by multiple ion implants with ^{31}P or ^{75}As (in place of ^{10}B) obtaining 3×10^{18} , 1×10^{19} , and 4×10^{19} atom/cm³ backgrounds with similar level of concentration homogeneity as in the ^{10}B one. As an example in Fig. 1 the ^{10}B , ^{11}B , and C profiles are shown together with an indication of the amorphous crystalline (a/c) interfaces after amorphization.

The structures were then recrystallized through solid-phase epitaxy (SPE) induced by rapid thermal annealing at 700 °C with the minimum thermal budget needed to get a complete regrowth in order to minimize the broadening of the B delta after recrystallization. The total time needed to obtain complete recrystallization for different doping profiles were calculated according to Ref. 23. Complete regrowth was checked by means of high-resolution x-ray diffraction. Moreover the amount of strain induced by the doping background and by the $\text{Si}_{1-x}\text{C}_x$ box was accurately evaluated by

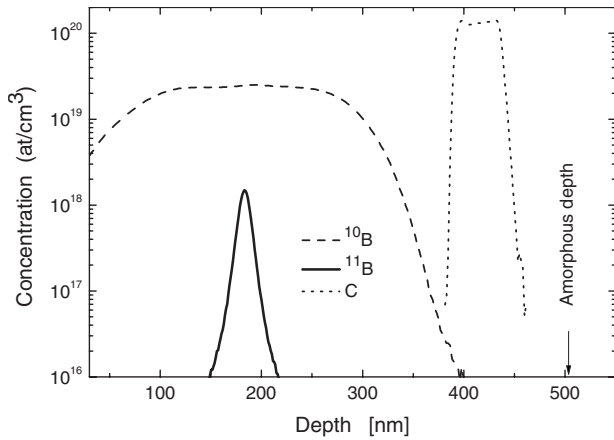


FIG. 1. SIMS concentration profiles of the ^{10}B background, the ^{11}B delta peak, and the $\text{Si}_{1-x}\text{C}_x$ box (dashed, continuous, and dotted lines, respectively). They are obtained after MBE growth, amorphization, and background implants. The arrow indicates the amorphous/crystal interface after amorphization implant.

the same technique and compared with literature data relative to substitutional P, B, and C.^{24–26} This allowed to verify that all these three elements are fully substitutional after regrowth for all the produced samples. As far as the arsenic-doped samples are concerned, the strain induced by this element is very low. Therefore Rutherford backscattering spectroscopy channeling was used to test its substitutionality, obtaining that 1×10^{19} As/cm³ sample is fully substitutional (and therefore very reasonably this can be assumed also for the 3×10^{18} As/cm² sample) while the 4×10^{19} As/cm³ sample has only 85% substitutional As. Therefore this sample was excluded by the following diffusion analyses.

Annealings to induce a moderate diffusion of the spike, suitable for λ and g determination, were then performed at temperatures between 530 and 810 °C for several times, ranging from 100 s to 230 h. More in details, the B background sample and a sample without the background were annealed at different temperatures in order to explore the temperature dependence of the parameters in Eqs. (1)–(3) while n -doped samples were annealed at 700 °C in order to extend the model in n -doping regime.

The substitutional C in the $\text{Si}_{1-x}\text{C}_x$ alloy layer prevents the I flux produced by the end-of-range defects dissolution from reaching the B delta and inducing I -related nonequilibrium diffusion phenomena, as previously described.^{9,27,28} We verified by high-resolution x-ray diffraction, that the amount of substitutional C in our samples is enough to avoid any I 's supersaturation since about 90% of C is still in substitutional sites even after the longest annealing. We also verified that B, As, and P backgrounds are fully substitutional after the annealing demonstrating that all the diffusion phenomena are not influenced by precipitation or clustering.

The annealings were performed by means of two apparatus. Annealings shorter than about 45 min were performed in a rapid thermal annealing Jipelec Jetfirst 150 with heating and cooling rates higher than 50 °C/s. The samples were mounted on a silicon 6 in. wafer, and lamps heating was controlled by a feedback on a pyrometer mounted on the wafer backside. The pyrometer was previously calibrated us-

ing a commercial silicon wafer with a high-precision thermocouple glued on the back. An independent check of the temperature calibration was made by measuring the solid-phase epitaxial regrowth rate of an amorphized silicon layer and the oxidation rate of silicon. The whole error on the temperature is ± 5 °C.

The longer annealings were performed in a GERO conventional tubular furnace placing the sample in a quartz open ampoule. Samples are inserted in the furnace after that the work temperature was reached, reducing the heating ramps to few minutes. The temperature was calibrated by a couple of high-precision thermocouples and verified by means of SPE and oxidation standard treatments giving an error of ± 5 °C. Moreover a cross-check among the two annealing apparatus was performed by comparing the diffusion of two sample with a 45 min treatment obtaining an agreement within the above errors. All the annealings were performed in N_2 high-purity atmosphere.

In order to provide λ and g determination with high accuracy and sensitivity the profiling technique is crucial. We performed secondary-ion mass spectrometry (SIMS) measurements with a Cameca IMS 4f, using a 3 keV O_2^+ beam and collecting B^+ secondary ions.

A particular measurement protocol was adopted by freezing the sample at -70 °C during the analysis. As previously demonstrated, low temperature prevents measurement artifacts due to long-range room-temperature diffusion phenomena of B induced by the point defects injected by the sputtering beam.²⁰ Moreover, we flooded the samples during the analyses with a jet of O_2 gas as described in Ref. 29. This allows to considerably increase (up to a factor of 20) the B^+ yield (some 10^4 counts/s are collected on the top of the delta) while maintaining the suppression of sputtering-induced migration phenomena, and without any loose of depth resolution.²⁹ As a consequence of the whole procedure, the errors for determining the diffusion g and λ diffusion parameters are, respectively, a factor of about six and three lower than for standard measurement conditions, i.e., at room temperature and in ultrahigh vacuum.

III. TEMPERATURE DEPENDENCE IN INTRINSIC AND p -DOPING REGIME

A. Results

In order to investigate the temperature dependence of the parameters regulating the B diffusion in intrinsic and p -doping regime we performed annealings on a sample without background and a sample with a 2.8×10^{19} B/cm³ background. The temperature range between 610 and 810 °C was investigated for the sample without the background while, thanks to the higher diffusivity, it was possible to reduce the temperature down to 530 °C in the sample with the background with a maximum annealing time of 230 h. With the exception of this last sample, 2 or 3 annealing times for each temperature were performed. All the samples were measured by SIMS with the above-described protocol.

As an example, Fig. 2 shows two profiles of samples without background and annealed at different temperatures (circles for 610 °C and triangle for 810 °C) compared to the

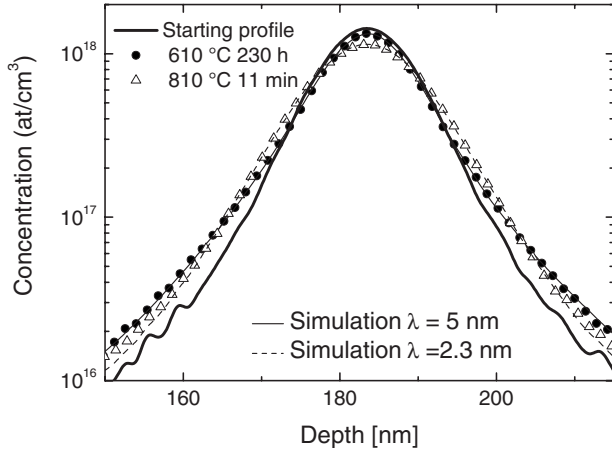


FIG. 2. Experimental B profile of the delta marker after the solid-phase epitaxy process (starting profile, thick solid line), after 230 h of annealing at 610 °C (circles) and after 11 min at 810 °C (triangles). The corresponding simulations are also reported (continuous and dashed line, respectively). Note the different shape of the two diffused profiles due to different B_I mean-free-path values.

starting profile (thick solid line). Even if the diffusion is very small, the two diffused profiles, have different shapes: the concentration of the 610 °C sample (compared to the 810 °C sample) is higher on the top of the profile and lower at an intermediate concentration and again higher on the tails.

In order to extract D , g , and λ parameters all the profiles were fitted by numerically “diffusing” the B profile of the sample just after SPE by the equations regulating the I -mediated diffusion described in Refs. 4, 5, and 18. An automatic chi-square optimization allowed to determine the parameters and their statistical error. The dashed and thin solid lines in Fig. 2 represent the best fit of the data by means of the procedure described above. The different shape of the two profiles can now be explained by considering that the two samples have very different λ values: 5.2 nm for the lower temperature and 2.2 nm for the higher one. Therefore, in the first case a more pronounced tailing is visible while in the second case the shape is closer to a Gaussian diffusion that would be the limit case for $\lambda=0$.

In Figs. 3(a) and 3(b) all the obtained diffusivity D and mean-free-path λ data are reported in an Arrhenius plot. Open circles are relative to the 2.8×10^{19} B/cm³ background while the close squares regard the sample without any background. We remark that all the information obtained by the experimental data is reported in these two panels since g values can be derived by the Eq. (4) from D and λ values. The choice of presenting D and λ among the three parameters D , λ , and g was driven by their lower statistical error and their clearer and more direct physical interpretation.

General considerations can be made on these experimental data. First of all, as expected, the diffusivity data for highly doped sample are greater than the data without any background, in agreement with the Fermi-level effect described by Eq. (2). Moreover, some samples show a quite large spreading of the diffusivity values. This is particularly evident for data concerning the 610 and 640 °C for the

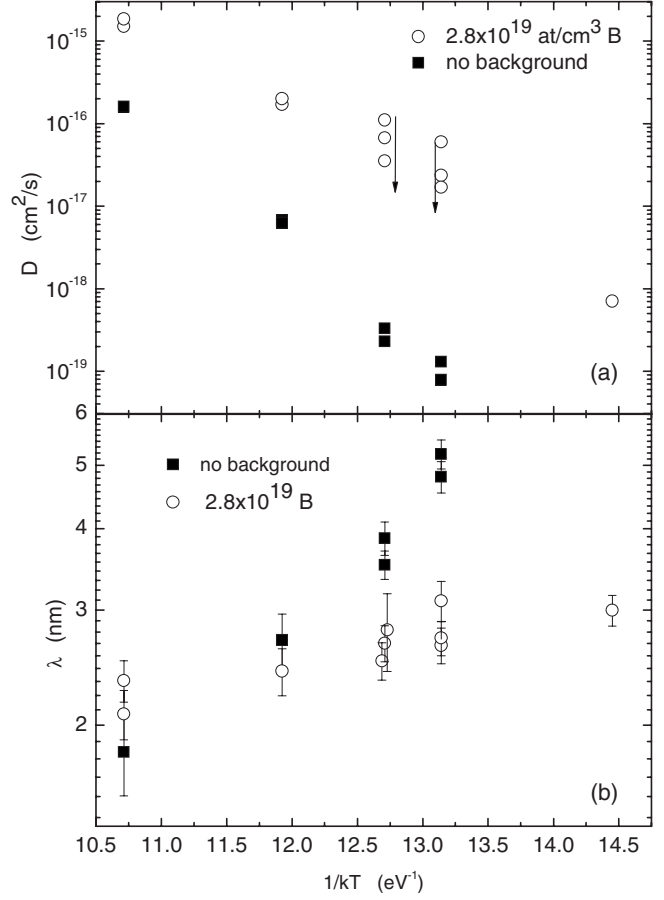


FIG. 3. Diffusivity (upper panel) and mean-free-path (lower panel) data as a function of $1/kT$ for the samples with and without B background (open and closed symbols, respectively). The arrows indicates data deduced by samples with increasing annealing times.

p -doped sample ((kT^{-1}) equal to about 13 and 12, respectively). This spreading is bigger than the estimated error that is of about 20% (as calculated by considering statistical fluctuations and temperature errors). More in detail such a spreading is related to a decrease in diffusivity by increasing the annealing time. On the contrary λ values are well reproducible at a fixed temperature within the error bars and do not change with the annealing time. Therefore, given the Eq. (4), this transient behavior is related to the frequency with which B reacts with I (g) and not to the mean-free path traveled by the mobile complex.

The above trend is somewhat expected. Transient diffusion phenomena in epitaxial systems are well known and are generally due to the presence of grown-in defects that modify the equilibrium populations of point defects.³⁰ In other words it is known that during the growth a small amount of point defects is embedded in the crystal and the system needs a transient time to anneal such defects and to reach the equilibrium. In our case, the amorphization step should eliminate the MBE grown-in defects, if any, but the following SPE process might introduce other defects. Generally epitaxy at high temperature is preferred in order to establish equilibrium in point defects populations. This is one of the reasons why we choose a relatively high SPE temperature (700 °C) for all our samples, and the other one is that,

the transient phenomena due to grown-in defects are expected to have a larger effect at lower temperatures where the equilibrium population of point defects are lower and the grown-in defect annihilation is slower. Moreover, the deviation from equilibrium population should induce a change in the B-I encounter frequency but not (on a first order) in the BI diffusion and stability i.e., it should not change λ in perfect agreement with the present observations. It is somewhat unexpected that transients are much more evident in p -doped samples since in these systems the I equilibrium population is larger. On the other hand, B increases SPE velocity and this might produce samples with a higher amount of grown-in defects. In addition to the above phenomena we cannot exclude that also not complete trapping efficiency of interstitials coming from end-of-range defects by C-rich layer might occur producing an additional contribution to the transient effects.

As a summary we can conclude that highly B-doped samples at temperature less or equal than 640 °C (the three data groups with open circles at higher $1/kT$) are not reliable as far as it concerns the diffusivity values while all the λ values are good since they are not affected by transient effects problems. On the contrary all data with no background (both D and λ) will be considered for the following analysis.

B. Data analysis

Figure 4(a) shows the diffusivity data divided by the $\langle p/n_i \rangle$ values for both samples with and without a constant background, with the exclusion of constant background samples at temperatures equal or below 640 °C. $\langle p/n_i \rangle$ values are obtained as briefly described in the Appendix. If Eq. (2) holds, the diffusivity divided by $\langle p/n_i \rangle$ should represent the $D_{B/I0}$. In other words the plot of Fig. 4 allows to evaluate the temperature trend of the diffusion component through the neutral BI species. As can be noted all the data fall to a good approximation on a single Arrhenius plot with an activation energy and a prefactor of $10^{0.3 \pm 1.3} \text{ cm}^2/\text{s}$ and $3.45 \pm 0.25 \text{ eV}$, respectively.

A second step of analysis permits to determine activation energies and prefactor for g_{I0} and g_{I++} . To do this we formulate the following working hypothesis that can be self-consistently tested at the end of the analysis. We suppose that I^0 -mediated diffusion always dominates diffusion for the samples without background at all temperatures, i.e., we suppose that $g_{I0} \gg g_{I++} \langle p/n_i \rangle^2$. Under these hypotheses, Eqs. (1)–(3) can be written as

$$\frac{g_{I0}}{D_{B/I0}} = \frac{1}{\lambda^2} \frac{p}{n_i}. \quad (7)$$

It is therefore possible to determine the ratio between g_{I0} and $D_{B/I0}$ directly on the basis of the experimental values of λ and on the calculated values of $\langle p/n_i \rangle$. Such ratio is reported in Fig. 4(b) with close symbols as a function of $1/kT$. A good Arrhenius trend is obtained and fitted with an activation energy of $0.65 \pm 0.10 \text{ eV}$ and a prefactor equal to $10^{2.7 \pm 0.6} \text{ nm}^{-2}$.

The data relative to p -doping background can be treated in a similar way in order to obtain the energetics of I^{++} dif-

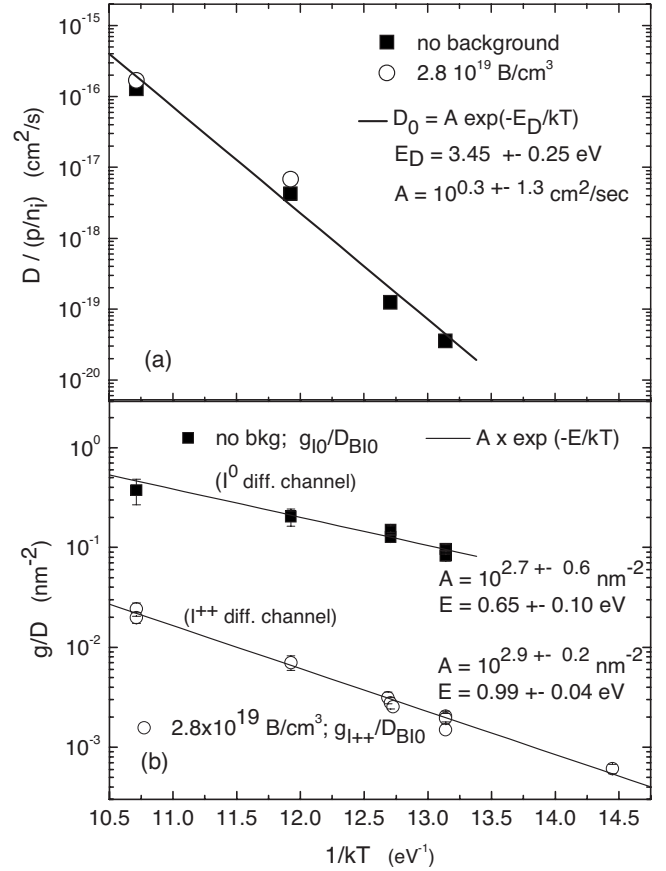


FIG. 4. Diffusivity normalized by the relative hole concentration as a function of $1/kT$ (upper panel). In the lower panel, the mean-free-path data are normalized according to the Eqs. (7) and (8) giving the $g_{I0}/D_{B/I0}$ (close symbols) and $g_{I++}/D_{B/I0}$ model parameters as a function of $1/kT$.

fusion channel. Equation (3) can be rewritten as

$$\frac{g_{I++}}{D_{B/I0}} = \frac{1}{\lambda^2} \left(\frac{p}{n_i} \right)^{-1} - \frac{g_{I0}}{D_{B/I0}} \left(\frac{p}{n_i} \right)^{-2}. \quad (8)$$

Therefore the $g_{I++}/D_{B/I0}$ ratio can be obtained directly by λ values of the p -doped samples [i.e., first term of right member of Eq. (8)], taking into account the correction due to I^0 channel [second term of the right member of Eq. (8)]. Actually this correction plays a small role only at 810 °C, where p/n_i is relatively low (about 11). At this temperature the correction is comparable to the experimental error while it is completely negligible at lower temperatures.

In Fig. 4(b) the λ experimental data of the p -doped samples are elaborated according to the second member of Eq. (8) and plotted as open circles. As can be noted the data can be well fitted by an Arrhenius curve with activation energy of $0.99 \pm 0.04 \text{ eV}$ and a prefactor equal to $10^{2.9 \pm 0.2} \text{ nm}^{-2}$.

At this level, the determined values of $g_{I++}/D_{B/I0}$ and $g_{I0}/D_{B/I0}$ can be used to test the initial hypothesis that $g_{I0} \gg g_{I++} \langle p/n_i \rangle^2$ for no-background samples. It can be verified that this holds true always well outside the experimental error demonstrating the self-consistency of the above data re-

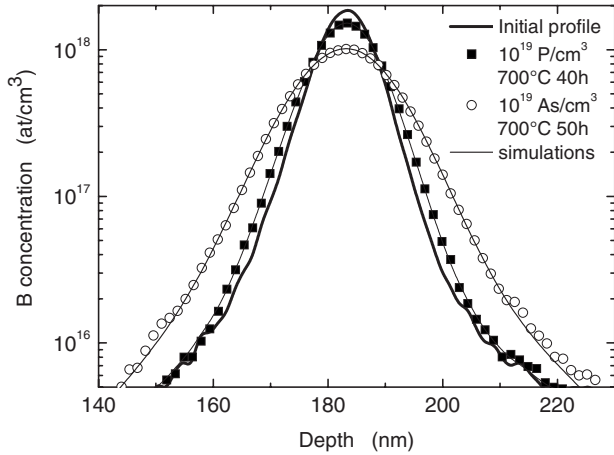


FIG. 5. Starting (thick line) and diffused concentration profiles under n -doping conditions (10^{19} atom/cm²). Open symbols are related to an As-doped sample. Close symbols come from a P-doped sample. Thin lines are the corresponding simulations.

duction. As a final remark we make notice that the present analysis, providing the ratios $g_{I^{++}}/D_{B/0}$ and $g_{I^0}/D_{B/0}$, is exclusively based on λ values that are accurate parameters since they are not affected by the transient phenomena.

IV. DIFFUSION IN n -DOPING REGIME

A. Results

In the present section the results reported above for intrinsic and p -doping conditions will be extended to the n -doping regime. To this aim As and P backgrounds were introduced into the samples as described in Sec. II.

Figure 5 shows the diffusion of two deltas having P (squares) and As (circles) 1×10^{19} atom/cm³ backgrounds annealed at 700 °C for similar times (40 and 50 h, respectively). Even if the two samples have the same doping level (both samples are demonstrated to have full substitutional, i.e., active doping), and therefore the same Fermi-level position they undergo a very different diffusion process. Therefore, Fermi-level position is not the only parameter regulating B diffusivity in n doping but chemical effects must be considered.

Continuous lines are fits to the data in order to determine D , g , and λ as done previously. Best fits are obtained with very similar λ values of about 1.1 ± 0.2 nm. The small, but not null, λ value accounts for the quasi-Gaussian diffusion and is confirmed by the analysis of other annealing times. Moreover, relatively small transient effects (on the order of 30%) on the diffusivity were observed for n -doped samples.

D , g , and λ values obtained from the above profiles are reported in Fig. 6, together with other data extracted from different n -type backgrounds at 700 °C and the data published previously in Ref. 18 with and without B backgrounds. The D and g data relative to the longest annealing times are reported in order to minimize the transient effects while the λ values are averaged over different times to reduce the statistical errors. p/n_i is calculated as described in the Appendix. With the new data p/n_i extends from

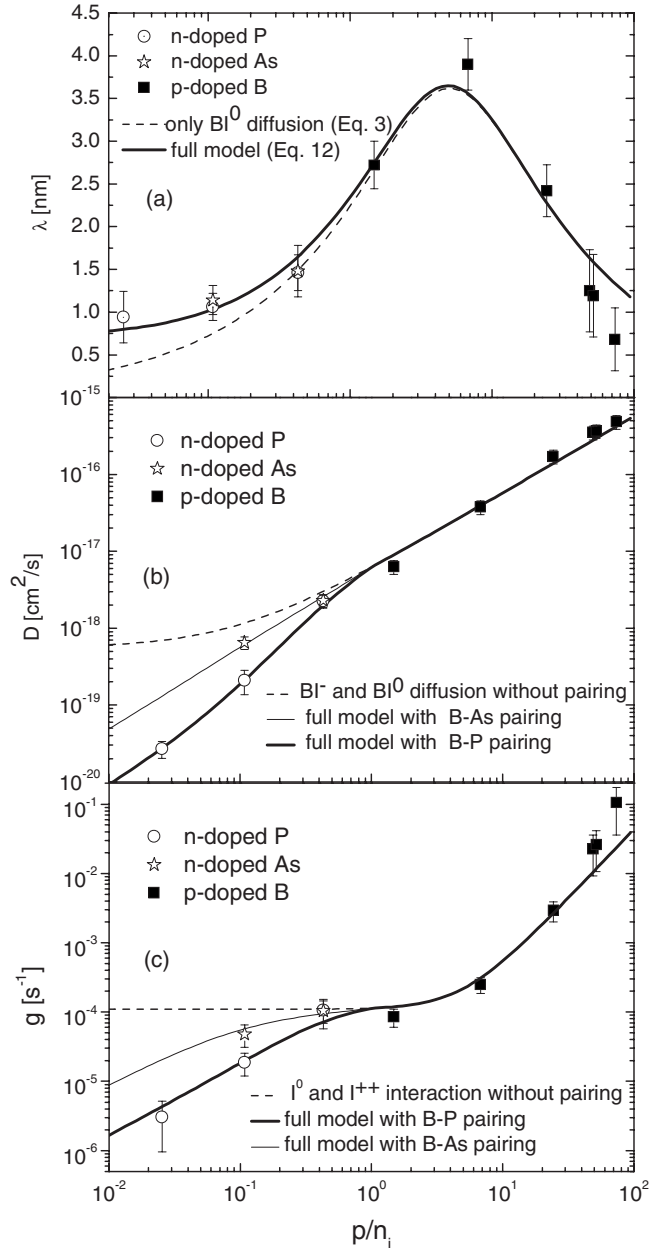


FIG. 6. Mean-free path, diffusion, and kick-out frequency (panels a, b, and c, respectively) as a function of the hole concentration normalized to the intrinsic carrier concentration at 700 °C. Squares are related to B-doped samples, stars to As-doped, and circles to P-doped one. Thick lines are the full model [Eqs. (10)–(12)] fit to the data, taking into account both BI^- diffusion and P-B pairing (thin line is obtained considering B-As pairing). Dashed line in top panel shows what happens by neglecting BI^- diffusion while dashed line in middle and bottom panels shows what happens if pairing is neglected and only BI^- diffusion is considered. Only by considering both phenomena all the experimental data can be reproduced.

2.5×10^{-2} to 75, i.e., over more than 3 orders of magnitude.

As can be noted λ values of Fig. 6(a) are all the same for a given p/n_i value independently of the doping species while g [Fig. 6(c)] and consequently D [Fig. 6(b)] split into two different trends for n -doping regime depending on the dop-

ing element. Dashed lines in Figs. 6(a) and 6(c) are the extension into n -doping regime of the model described by the Eqs. (1) and (3) for λ and g without any modification. The model provides a good fit only at moderate n -doping regime with $p/n_i \geq 0.4$ while it is not able to describe the deep n -doping regime. Also a pure linear D trend as proposed in Eq. (2) [not shown in the Fig. 6(b)] cannot fit all the data (especially those with phosphorus doping) for $p/n_i < 0.4$. The above considerations clearly demonstrate that additional phenomena with respect to the model embedded in Eqs. (1)–(3) should be considered.

B. Data analysis

The first phenomenon that has to be considered in n regime is the pairing that occurs between oppositely charged B and As (or P) due to Coulomb attraction. This phenomenon is a general effect that occurs when n and p codoping is performed in a semiconductor. A series of experimental papers demonstrated that donors and acceptors tend to be located in first nearest-neighborhood substitutional sites stabilized by Coulomb attraction.¹ Such attraction lowers the energy of substitutional atoms and therefore increases the energy needed to move those atoms to diffusive configurations. On the other hand, theoretical papers have suggested that also BI^- species may be mobile. If this was true, the contribution to diffusivity of this species would be constant as a function of p/n_i , and would be more and more visible at low p/n_i , where the linear contribution of BI^0 is depleted.

In general, as well demonstrated in Ref. 1, it is quite difficult to disentangle the effects of ion pairing and the effect of BI^- diffusion on the basis of the D experimental data alone as they have opposite effects on D and can compensate each other. In the following, we will show how this can be done efficiently by investigating all the diffusion parameter D , g , and λ of B diffusion in n -doping regime.

An impurity atom involved in the formation of a pair needs an additional energy (with respect to an unpaired atom) to realize its diffusion path and this energy is equal to the Coulomb pairing energy. Given a typical Coulomb barrier of 0.5 eV this makes the diffusion contribution due to impurities in pairs negligible. In fact diffusion is decreased by a factor $\exp(-0.5/kT)$, that is, for the temperatures adopted in this experiment, less than 1%. The diffusion flux associated with the unpaired p -type atoms can be written as

$$\varphi = D \frac{\partial(c_p - c_{Pair})}{\partial x} = D \frac{\partial(c_p - c_{Pair})}{\partial c_p} \frac{\partial c_p}{\partial x}, \quad (9)$$

where c_p is the p -type impurity total concentration, c_{Pair} is the concentration of pairs, and D is the diffusion coefficient in absence of pairing. The measured diffusivity, when pairing is acting, results to be the diffusivity without pairing multiplied by the factor $f = \partial(c_p - c_{Pair}) / \partial c_p$. Under equilibrium conditions this last factor can be evaluated by a free-energy minimization according to the equation,¹

$$f = \frac{1}{2} \left(1 + \frac{c_p - c_n + \frac{c_{Si}}{4} e^{-E_{Pair}/kT}}{\sqrt{\left(c_p - c_n - \frac{c_{Si}}{4} e^{-E_{Pair}/kT}\right)^2 + c_{Si} c_p e^{-E_{Pair}/kT}}} \right), \quad (10)$$

where c_n is the n -type dopant concentration, c_{Si} is the silicon density, and E_{Pair} is the energy gain due to ion-pairing interaction. By combining Eq. (10) and Eq. (A1) of the Appendix, it is possible to express the fraction of paired B atoms as a function of p/n_i .

On the other hand, ion pairing is not expected to influence the atomistic parameter λ if the average distance between B and P (or As) atoms is larger than λ itself. In this case the mean-free path would be unperturbed by the B capture by P or As. This approximation is valid in the considered system since it can be evaluated that the average B-P (or B-As) distance is at least 2–3 times higher than the measured mean-free paths.

Therefore while the pairing can be invoked in order to describe the reduction in D at high n doping it cannot explain the increase in λ with respect to the previous model. More in details, according to the previous version of the model, BI^0 should be the only mobile species and therefore when p/n_i goes to zero, no holes are available to transform BI^- into BI^0 and therefore the mean-free path should go to zero. The scenario changes if a small BI^- diffusivity is considered: in this case a finite mean-free path can exist also in absence of holes.

The above considerations make us to conclude that the diffusivity should be described by

$$D = f(p/n_i, E_{Pair}, T) \left(D_{BI^-} + D_{BI^0} \frac{p}{n_i} \right), \quad (11)$$

where both pairing reduction and BI^- contribution are considered.

On the other hand λ should be modified to

$$\lambda = \sqrt{\frac{D_{BI^-} + D_{BI^0} \frac{p}{n_i}}{g_{I0} + g_{I++} \left(\frac{p}{n_i}\right)^2}}, \quad (12)$$

where Eq. (3) has been upgraded accordingly by adding the D_{BI^-} contribution but correctly it does not present any effect due to pairing. In this new formulation, the limit of λ as p/n_i approaches zero is D_{BI^-}/g_{I0} that is finite and regulated by the new D_{BI^-} parameter.

As a consequence of the Eqs. (4), (11), and (12) the measured kick-out frequency must be described by

$$g = f(p/n_i, E_{Pair}, T) \left[g_{I0} + g_{I++} \left(\frac{p}{n_i}\right)^2 \right]. \quad (13)$$

Equations (11)–(13) [together with the definition of f by Eqs. (10) and (A1)] are therefore an extension of the diffusion model to the n -doping regime. The new model is used to obtain a fit to the data that is reported by the continuous lines

in Fig. 6. The fit can be obtained by a single set of the parameters involving pairing (i.e., B-P and B-As pairing energies) and the BI^- diffusion parameter (D_{BI^-}). The two energies modify the trend of g significantly, without any consequence on λ while D_{BI^-} modifies the λ trend leaving g unchanged. At the end, the very good fit fixes independently all the new physical parameters and let unchanged the model in p -type regime where it merges with the model obtained previously for the p -type regime.

V. SUMMARY AND DISCUSSION

Equations (11)–(13) and [together with Eq. (10) that allows to calculate f] are a single analytical model that describes the trend of the diffusivity and the mean-free path as a function of free-carrier concentration. The three equations can be rearranged in a more practical form as follows:

$$D = D_{B/I0} \left(\frac{p}{n_i} + \frac{D_{BI^-}}{D_{B/I0}} \right) f(p/n_i, E_{\text{pairing}}, T), \quad (14)$$

$$\lambda = \left[\frac{1 + \frac{D_{BI^-}}{D_{B/I0}} \left(\frac{n_i}{p} \right)}{\frac{g_{I0}}{D_{B/I0}} \left(\frac{n_i}{p} \right) + \frac{g_{I++}}{D_{B/I0}} \left(\frac{p}{n_i} \right)} \right]^{1/2}, \quad (15)$$

$$g = \frac{D}{\lambda^2}. \quad (16)$$

This form allows to evidence the connection with the parameters determined in the experiments described in the above sections that are

$$D_{B/I0} = 10^{0.3 \pm 1.3} e^{-(3.45 \pm 0.25) \text{ eV}/kT} \text{ cm}^2/\text{s}, \quad (17)$$

$$\frac{D_{BI^-}}{D_{B/I0}} = (0.09 \pm 0.05) \text{ (at } 700 \text{ }^\circ\text{C)}, \quad (18)$$

$$E_{BP} = 0.75 \pm 0.08 \text{ eV}, \quad (19)$$

$$E_{BP} - E_{BAS} = 0.14 \pm 0.07 \text{ eV}, \quad (20)$$

$$\frac{g_{I0}}{D_{B/I0}} = 10^{2.7 \pm 0.6} e^{-(0.65 \pm 0.10) \text{ eV}/kT} \text{ nm}^{-2}, \quad (21)$$

$$\frac{g_{I++}}{D_{B/I0}} = 10^{2.9 \pm 0.2} e^{-(0.99 \pm 0.04) \text{ eV}/kT} \text{ nm}^{-2}. \quad (22)$$

Equations (14)–(22) represent a full model experimentally based able to predict B diffusion shape in a large range of doping conditions and temperatures.

The main diffusion mechanism dominating in intrinsic and p -doping regime is through BI^0 species. Prefactor and activation energy of $D_{B/I0}$ [Eq. (17)] fall about in the middle of the relatively large distribution of all the data obtained in the past.¹ Moreover, the data are in fair agreement with recent data of Bracht and co-workers¹⁹ that determined the

diffusivity at temperatures higher than the temperature range investigated by us (850–1100 °C instead of 610–810 °C). While prefactor and activation energies are in good agreement within the error bars, our data are slightly higher if compared to the extrapolation of Bracht data. This is very probably due to systematic errors because of the use of different experimental methodologies and not to physical reasons. In particular, our data could be affected by a nonfull correction of transient effects.

On this basis it can be very reasonably stated that a single dominating diffusing process acts from 610 to 1100 °C demonstrating that BI^0 diffusing species dominates the diffusion in a very large range of temperatures. This is a nontrivial result that extends the I -mediated mechanism [up to now demonstrated for temperatures higher than 810 °C (Ref. 6)] to significantly lower temperatures.

A second diffusion channel, that becomes important only in n -doping regime, is mediated by the BI^- species. In particular, D_{BI^-} (i.e., contribution to diffusion of BI^- species in intrinsic condition) is about 9% of $D_{B/I0}$. It is worth to note that Windl and co-workers¹⁵ already predicted such a contribution in n regime that is now experimentally evidenced. Estimation of D_{BI^-} activation energy is not performed in the present work. On the other hand, a rough estimate of the D_{BI^-} trend with temperature can be obtained on the basis of the present data assuming that D_{BI^-} and $D_{B/I0}$ have the same prefactor. In this way the D_{BI^-} activation energy results to be $E_{BI^-} = 3.65$ eV, i.e., there is an increased energy cost for BI^- diffusion with respect to BI^0 diffusion of about 0.20 eV. This is in reasonable agreement with *ab initio* calculations by Windl *et al.* that predicted an increase of 0.14 or 0.02 eV with, respectively, GGA and LDA approaches.¹⁵

As far as the pairing is concerned, the pairing energies we obtained [Eqs. (19) and (20)] are very reasonably close to a simple Coulomb interaction between first neighborhood sites (about 0.5 eV). In particular, P-B pairing energy is somewhat higher than what was previously estimated (0.56 eV according to Fair and Pappas,¹¹ 0.7 ± 0.2 eV according to Cowern *et al.*,³¹ or 0.44 eV according to Wittel and Dunham³²). This is not surprising since these estimates are based on the assumption that BI^- diffusion contribution is not present and a pairing effect, stronger than what was previously determined, is necessary to compensate the BI^- diffusion contribution.

Concerning instead the role of arsenic Fair and Pappas¹¹ stated that As induces the same diffusion reduction in P at the same concentration. This is clearly in contradiction with our observation (see Fig. 5). Moreover, a number of publications invoked the formation of a B-As mobile complex that influences diffusion.^{33–35} All these last results are obtained with a very high As concentration of about 1×10^{20} atom/cm³. As mentioned in the experimental section even a 4×10^{19} atom/cm³ As concentration (not considered for diffusion in this paper), is not completely substitutional after the regrowth annealing. Therefore it is quite reasonable that the above literature results are affected by phenomena involving As in not substitutional sites and they are not comparable to the simple B-As pairing occurring in our fully substitutional As background samples.

The physical processes underlying the model are numerous and complex. In Fig. 7 all the processes are represented

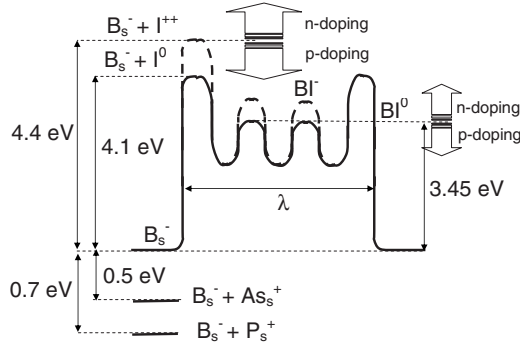


FIG. 7. Energy scheme of B diffusion. Substitutional B (B_s^-) can move by interaction with I^0 or I^{++} with energy barrier for mobile species generation of 4.1 and 4.4 eV, respectively. The BI species moves through negative BI^- or neutral BI^0 saddle points. This last is the main mechanism and it causes a 3.45 eV total activation energy for diffusion. The binding energy of substitutional B with As or P n dopant is also indicated. The paired B undergoes a strong increase in the diffusion energy cost. Arrows indicate the movement direction of BI^0 and I^{++} energy levels as a function of doping.

by energies barriers related to the different physical mechanisms involved. The scheme is referred to intrinsic conditions, arrows indicate the major effect of extrinsic doping. The basic diffusion process occurs with an energy cost that is the difference between the energy of the saddle point of diffusion of the BI species and the energy of the substitutional B atom. Two possible channels are evidenced through BI^- or BI^0 but the last one is more convenient. By changing the free-carrier concentration the energy difference between B_s^- and BI^- remains unchanged, since the two species have the same charge but the barrier for BI^0 changes, causing the dependence of D on (p/n_i) in our model. Moreover, the introduction of n dopant lowers the starting energy level of substitutional B through the formation of pairs, which force a fraction of B atoms to have a much higher-energy cost for diffusion.

The scheme also describes the precise paths by which BI complexes are formed, that determines the trends of g and λ . Two possible paths are evidenced, one through I^{++} and the other through I^0 . In intrinsic conditions the I^0 path is much more convenient but, by moving toward p -doping conditions I^{++} formation becomes favored as its energy cost reduces [this fact causes the $(p/n_i)^2$ term in g trend] and it becomes the dominant I species causing diffusion.

In the scheme of Fig. 7 the activation energies for g_{I^0} and $g_{I^{++}}$ are reported [they can be easily deduced by Eqs. (20), (21), and (16)]. Such energies are 4.1 and 4.4 eV, respectively; while the prefactors are both about 10^{17} s^{-1} . Generally the B-I reaction frequency g is considered to linearly depend upon the concentration of I s (c_I), their diffusivity (D_I), and the capture radius (a) below which B-I interaction occurs,

$$g = 4\pi a D_I c_I. \quad (23)$$

If a constant and “lattice related” capture radius is considered (i.e., $a=0.543 \text{ nm}$) g_{I^0} and $g_{I^{++}}$ would be directly related to the transport capacity ($D_I c_I$) of I^0 and I^{++} defects,

respectively. Different evaluation of these fundamental parameters are reported in literature, and as far as it concerns theoretical determination a large spreading is observed but in general the agreement is quite good with those calculations that do not apply energy-gap-related corrections.²¹ As far as experimental determinations are concerned the most recent ones are related to the determination of the Si self-diffusion D_{Si} , that is related to the I transport capacity through

$$D_{Si} = \xi_I D_I c_I + \xi_V D_V c_V, \quad (24)$$

where $D_V c_V$ is the vacancy self-diffusion and ξ_I and ξ_V are the correlation factors for interstitials and vacancies, respectively. The Eq. (24) is a simplified one since a sum over the different charge states for both vacancies and interstitials must be considered. Combining self-diffusion and dopant diffusion data Bracht and co-worker determined both B diffusion coefficient and I transport capacity in p -doping regime in the temperature range between 850 and 1100 °C. In general, agreements between the two independent methodologies can be evidenced. In both cases only BI^0 diffusion channel is necessary to fit p -doped species. Moreover, it can be calculated by Ref. 19 data that I^+ interstitial contribution to g is always less than 10% at every experimental temperature in intrinsic and p -doping condition, confirming that the dominant channel are through I^0 and I^{++} . Activation energies and prefactor for diffusion of BI^0 channel are in good agreement. Putting together the two set of results allows to assert that the paths of dopant interaction with I and diffusion are the same in an extremely large temperature range between 530 and 1100 °C.

The agreement between the two sets of data is not complete. In fact the value for g that can be deduced by Bracht transport capacity data through Eq. (23) is always about one order of magnitude lower than what can be calculated by our data. Much higher activation energies for I^0 and I^{++} generation channels for BI are determined (4.96 ± 0.04 and $5.02 \pm 0.22 \text{ eV}$, respectively).

In order to relate this discrepancy to the experimental data, if we would try to fit Si self-diffusion data of Bracht *et al.* by means of the transport capacity deduced by our g values using relations (23) and (24) a much larger diffusion of the Si isotopically enriched marker would be obtained. On the contrary if Ref. 19 data are used to calculate λ , the profile of our delta-doped structure could not be reproduced. In particular, if we consider the profile of Fig. 2 at 810 °C, prediction of λ on the basis of Ref. 19 data should bring to a value about 6 nm similar to what we measure at a much lower temperature.

In order to deeper understand this discrepancy we think that only a cross experiment in which both the methodologies are exploited in a single sample could give a conclusive experimental picture. More in detail isoconcentration experiment with both boron and isotopically enriched Si delta could be performed to give directly comparable self-diffusion data and BI generation frequency values. We speculate that, if the present discrepancy would remain, it should reveal new physical aspects about diffusion in Si forcing to reconsider the largely used but not deeply tested hypotheses about capture radius and correlation factors [ap-

pearing in Eqs. (23) and (24)] that allow for the correlation between BI generation rate and I transport capacity. This information would furnish important element to the understanding of the structure and dynamic of I defects at high temperature.

VI. CONCLUSIONS

A unified model that quantitatively describes the atomistic mechanism of B diffusion in crystalline silicon is reported. In particular, we presented two experiments that allow to extend such description to a wide range of temperature and doping levels. Many physical processes are involved and all of them are demonstrated to play a role in order to correctly describe particular experimental features: (i) the diffusion of B atoms is started by the interaction with neutral and doubly positively charged interstitials; the kinetic of these reactions are fully characterized; (ii) in intrinsic and p -doping regime the BI complex diffuse through a neutral state of charge; (iii) an alternative pathway for diffusion is constituted by a negatively charged BI^- complex that becomes significant only in n -doping regime; (iv) BI^- diffusion and Coulomb pairing effects of B with n dopant (P and As) are disentangled and quantified.

The final quantitative model completes the existing literature and is in fair agreement with it. Moreover we evidenced that some of the more elusive quantitative parameters describing the scenario can reserve further discussions; they are the precise trend with the temperature of BI^- diffusion and the capture radii and correlation factors of self-interstitials.

APPENDIX

p/n_i calculation

In order to analyze the above data, it is fundamental to determine the (p/n_i) ratio at different B concentrations and temperatures. Once experimentally demonstrated that all dopants are fully substitutionally incorporated into the lattice, (p/n_i) can be computed on the basis of well-assessed literature data and methodologies. The n_i value is taken from Ref. 36 and varies from 1.5×10^{17} up to 2.6×10^{18} cm^{-3} in the investigated temperature range (530–810 °C). In the case of the sample with constant background, essentially no p gradient is present in the zone where the delta diffuses. The (p/n_i) calculation can be performed by taking into account Boltzmann statistics and considering a full ionization of sub-

stitutional B, as demonstrated in Ref. 37. Under these hypotheses, the following equation is adopted for (p/n_i) computing both for p - and n -doping backgrounds:

$$\frac{p}{n_i} = \pm \frac{c}{2n_i} + \sqrt{\frac{c^2}{4n_i^2} + 1}, \quad (\text{A1})$$

where c is the background concentration for p - or n -doping regime. The plus sign holds for p doping while the minus sign has to be used in the case of n -doping regime.

The scenario is a little bit more complicated when the background-free sample is considered. This case can be roughly thought as the “as much as possible” intrinsic case but, actually, a doping effect of the small delta has to be considered. In fact, the top concentration of the delta (about 2.0×10^{18} cm^{-3}) is always higher or comparable to the intrinsic carrier concentration. In the most favorable case, it is slightly lower (at 810 °C $n_i = 2.6 \times 10^{18}$ cm^{-3}) while in the worst one it is about five times bigger (at 610 °C $n_i = 4.1 \times 10^{17}$ cm^{-3}). In the background-free samples the carrier gradient due to inhomogeneous doping will cause hole diffusion that will be compensated by the appearance of an internal field generated by the net fixed charge of ionized B. p/n_i profile was calculated by solving the steady state of drift-diffusion equations together with Poisson equation for the field. Under the hypotheses that Einstein relation holds and hole and electron diffusivity are comparable, the p/n_i final profile only depends on temperature and on the B concentration profile. Such profile is in general quite flat over the dimension of the delta (not shown), allowing to determine a reasonable average p/n_i value through the formula

$$\left\langle \frac{p}{n_i} \right\rangle = \frac{\int \frac{p}{n_i}(z) c_B(z) dz}{\int c_B(z) dz}, \quad (\text{A2})$$

where z is the depth coordinate and c_B is the boron profile. The formula calculates the average value of (p/n_i) experienced by B along the depth. Of course this value changes as long as the B profile diffuses but an evaluation with the initial and final B profile differs of less than 3% in the worst case; in this way a negligible error is introduced. $\langle p/n_i \rangle$ has its higher and lower values at 610 and at 810 °C are 2.2 and 1.2, respectively. These are quite “intrinsic” values if compared with the values obtained for the constant background sample, that ranges from 70 at 610 °C up to 11 at 810 °C.

¹P. Pichler, in *Intrinsic Point Defects, Impurities, and Their Diffusion in Silicon*, edited by S. Selberherr (Springer, Wien, New York, 2004).

²P. M. Fahey, P. B. Griffin, and J. D. Plummer, *Rev. Mod. Phys.* **61**, 289 (1989).

³U. Goesele and T. Y. Tan, *Defects in Semiconductors II*, edited by J. W. Corbett and S. Mahayan (North-Holland, New York, 1983), p. 45.

⁴N. E. B. Cowern, K. T. F. Janssen, G. F. A. van de Walle, and D. J. Gravesteijn, *Phys. Rev. Lett.* **65**, 2434 (1990).

⁵N. E. B. Cowern, G. F. A. van de Walle, D. J. Gravesteijn, and C. J. Vriezema, *Phys. Rev. Lett.* **67**, 212 (1991).

⁶H. J. Gossmann, T. E. H. P. A. Stolk, D. C. Jacobson, G. H. Gilmer, J. M. Poate, H. S. Luftman, T. K. Mogi, and M. O. Thompson, *Appl. Phys. Lett.* **71**, 3862 (1997).

⁷S. C. Jain, W. Schoenmaker, R. Lindsay, P. A. Stolk, S. Decou-

- tere, M. Willander, and H. E. Maes, *J. Appl. Phys.* **91**, 8919 (2002).
- ⁸L. Pelaz, M. Jaraiz, G. H. Gilmer, H. J. Gossmann, C. S. Rafferty, D. J. Eaglesham, and J. M. Poat, *Appl. Phys. Lett.* **70**, 2285 (1997).
- ⁹S. Mirabella, A. Coati, D. De Salvador, E. Napolitani, A. Mattoni, G. Bisognin, M. Berti, A. Carnera, A. V. Drigo, S. Scalse, S. Pulvirenti, A. Terrasi, and F. Priolo, *Phys. Rev. B* **65**, 045209 (2002).
- ¹⁰D. De Salvador, E. Napolitani, G. Bisognin, A. Carnera, E. Bruno, S. Mirabella, G. Impellizzeri, and F. Priolo, *Appl. Phys. Lett.* **87**, 221902 (2005).
- ¹¹B. R. Fair and P. N. Pappas, *J. Electrochem. Soc.* **122**, 1241 (1975).
- ¹²M. Miyake, *J. Appl. Phys.* **57**, 1861 (1985).
- ¹³A. F. W. Willoughby, A. G. R. Evans, P. Champ, K. J. Yallup, D. J. Godfrey, and M. G. Dowsett, *J. Appl. Phys.* **59**, 2392 (1986).
- ¹⁴B. Sadigh, T. J. Lenosky, S. K. Theiss, M. J. Caturla, T. Diaz de la Rubia, and M. A. Foad, *Phys. Rev. Lett.* **83**, 4341 (1999).
- ¹⁵W. Windl, M. M. Bunea, R. Stumpf, S. T. Dunham, and M. P. Masquelier, *Phys. Rev. Lett.* **83**, 4345 (1999).
- ¹⁶J. W. Jeong and A. Oshiyama, *Phys. Rev. B* **64**, 235204 (2001).
- ¹⁷L. Lin, T. Kirichenko, B. R. Sahu, G. S. Hwang, and S. K. Banerjee, *Phys. Rev. B* **72**, 205206 (2005).
- ¹⁸D. De Salvador, E. Napolitani, S. Mirabella, G. Bisognin, G. Impellizzeri, A. Carnera, and F. Priolo, *Phys. Rev. Lett.* **97**, 255902 (2006).
- ¹⁹H. Bracht, H. H. Silvestri, I. D. Sharp, and E. E. Haller, *Phys. Rev. B* **75**, 035211 (2007).
- ²⁰E. Napolitani, D. De Salvador, R. Storti, A. Carnera, S. Mirabella, and F. Priolo, *Phys. Rev. Lett.* **93**, 055901 (2004).
- ²¹W. Windl and R. Stumpf, *Mater. Sci. Eng., B* **154-155**, 198 (2008).
- ²²W. Windl, *Appl. Phys. Lett.* **92**, 202104 (2008).
- ²³G. L. Olson and J. A. Roth, *Mater. Sci. Rep.* **3**, 1 (1988).
- ²⁴G. Celotti, D. Nobili, and P. Ostojica, *J. Mater. Sci.* **9**, 821 (1974).
- ²⁵G. Bisognin, D. De Salvador, E. Napolitani, M. Berti, A. Carnera, S. Mirabella, L. Romano, M. G. Grimaldi, and F. Priolo, *J. Appl. Phys.* **101**, 093523 (2007).
- ²⁶M. Berti, D. De Salvador, A. V. Drigo, F. Romanato, J. Stangl, S. Zerlauth, F. Schaffler, and G. Bauer, *Appl. Phys. Lett.* **72**, 1602 (1998).
- ²⁷U. Goesele, P. Laveant, R. Scholz, N. Engler, and P. Werner, *Si Front-End Processing Physics and Technology of Dopant-Defect Interactions II*, MRS Symposia Proceedings No. 610 (Materials Research Society, Pittsburgh, 2000), p. B7.1.1.
- ²⁸E. Napolitani, A. Coati, D. De Salvador, A. Carnera, S. Mirabella, S. Scalse, and F. Priolo, *Appl. Phys. Lett.* **79**, 4145 (2001).
- ²⁹E. Napolitani, D. De Salvador, M. Pesce, A. Carnera, S. Mirabella, and F. Priolo, *J. Vac. Sci. Technol. B* **24**, 394 (2006).
- ³⁰J. Christensen, A. Y. Kuznetsov, H. H. Radamson, and B. G. Svensson, *Appl. Phys. Lett.* **82**, 2254 (2003).
- ³¹N. E. B. Cowern, *Appl. Phys. Lett.* **54**, 703 (1989).
- ³²F. Wittel and S. Dunham, *Appl. Phys. Lett.* **66**, 1415 (1995).
- ³³K. Yokota, M. Ochi, T. Hirao, Y. Horino, M. Satho, Y. Ando, and K. Mutsuda, *J. Appl. Phys.* **69**, 2975 (1991).
- ³⁴K. Yokota, Y. Okamoto, F. Miyashita, T. Hirao, W. Watanabe, K. Sekine, Y. Ando, and K. Matsuda, *J. Appl. Phys.* **75**, 7247 (1994).
- ³⁵S. Solmi, S. Valmorri, and R. Canteri, *J. Appl. Phys.* **77**, 2400 (1995).
- ³⁶F. J. Morin and J. P. Maita, *Phys. Rev.* **96**, 28 (1954).
- ³⁷X. Luo, S. B. Zhang, and S. H. Wei, *Phys. Rev. Lett.* **90**, 026103 (2003).